Plasmonic mass and Johnson–Nyquist noise

2015 Nanotechnology 26 354002

(http://iopscience.iop.org/0957-4484/26/35/354002)

IOP Publishing Nanotechnology
Nanotechnology 26 (2015) 354002 (8pp) doi:10.1088/0957-4484/26/35/354002

Plasmonic mass and Johnson–Nyquist noise

Jingyee Chee[1], Hosang Yoon[1], Ling Qin[1] and Donhee Ham

School of Engineering and Applied Sciences, Harvard University, 33 Oxford Street, Cambridge, Massachusetts 02138, USA

E-mail: donhee@seas.harvard.edu

Received 18 March 2015, revised 1 June 2015
Accepted for publication 25 June 2015
Published 12 August 2015

Abstract

The fluctuation-dissipation theorem relates the thermal noise spectrum of a conductor to its linear response properties, with the ohmic resistance arising from the electron scattering being the most notable linear response property. But the linear response also includes the collective inertial acceleration of electrons, which should in principle influence the thermal noise spectrum as well. In practice, this effect would be largely masked by the Planck quantization for traditional conductors with short electron scattering times. But recent advances in nanotechnology have enabled the fabrication of conductors with greatly increased electron scattering times, with which the collective inertial effect can critically affect the thermal noise spectrum. In this paper we highlight this collective inertial effect—that is, the plasmonic effect—on the thermal noise spectrum under the framework of semiclassical electron dynamics, from both fundamental microscopic and practical modeling points of view. In graphene, where non-zero collective inertia arises from zero single-electron effective mass and where both electron and hole bands exist together, the thermal noise spectrum shows rich temperature and frequency dependencies, unseen in traditional conductors.

Keywords: plasmonics, noise, graphene, fluctuation dissipation theorem, linear response, kinetic inductance, plasmonic mass

(Some figures may appear in colour only in the online journal)

1. Introduction

The phenomenon of Johnson–Nyquist noise [1, 2] is not only of great importance for its own sake, but it also offers a prominent example of the fluctuation-dissipation relation [3, 4]. The fluctuation-dissipation theorem dictates that the power spectral density of the Johnson–Nyquist current noise in a conductor is given by [3, 4]

$$S_I(\omega) = 4k_B T \Re\{Y(\omega)\} \frac{\hbar\omega/k_B T}{\exp(\hbar\omega/k_B T) - 1}, \quad (1)$$

where $Y(\omega)$ is the complex admittance that represents the conductor's linear response. While the primary factor that affects $Y(\omega)$ is the ohmic resistance R arising from the electron scattering, $Y(\omega)$ must be a frequency-dependent, complex quantity, even in the most intrinsic case considering only the pure dynamical effects of electrons (i.e., even after excluding parasitic reactive elements). This is because the current response to an applied voltage entails not only the electron scattering but also the collective inertial acceleration of electrons, which manifests as a kinetic inductance L_K [5]. For a conductor with an arbitrary single-electron energy dispersion $\epsilon(\mathbf{k})$, L_K can be obtained by calculating the ac conductivity or dielectric function within the linear response framework [6–8]. In particular, the semi-classical approximation yields [6, 8]

$$L_K = \frac{l}{W}\frac{\hbar^2}{ge^2}\left[\int \frac{d^d\mathbf{k}}{(2\pi)^d}\frac{\partial^2\epsilon}{\partial k_x^2} f(\epsilon(\mathbf{k}))\right]^{-1}, \quad (2)$$

for a conductor with length l along the x-axis—along which $Y(\omega)$ and $S_I(\omega)$ are measured—and cross-sectional width or area, W, depending on conductor dimension $d = 2$ or 3. g accounts for degeneracy (e.g., due to spin and valley), and

[1] These authors contributed equally.

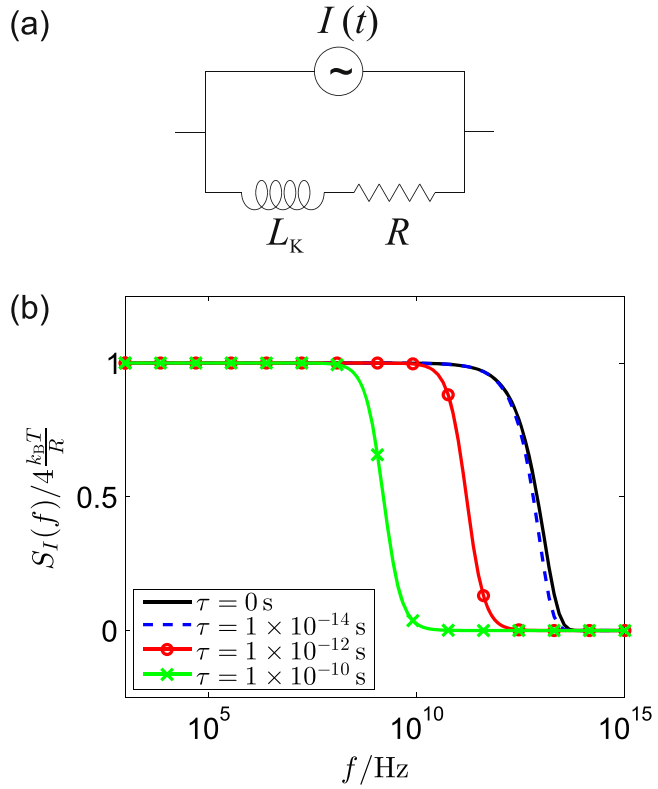

Figure 1. (a) Circuit model for the Johnson–Nyquist noise, including the kinetic inductance effect. (b) Current noise power spectral density for various τ values at $T = 300$ K.

$f(\epsilon) = [1 + \exp\{(\epsilon - \mu)/(k_BT)\}]^{-1}$ is the Fermi–Dirac distribution (μ: chemical potential). Then

$$Y(\omega) = \left(R + i\omega L_K\right)^{-1}, \tag{3}$$

with L_K and R in series. The corresponding circuit model is in figure 1(a). At low frequencies, equation (1) reduces to the familiar $4k_BT/R$. In the classical regime ($\hbar \to 0$), equation (1) reduces to

$$S_I(\omega) = 4k_BT\Re\{Y(\omega)\}. \tag{4}$$

Integrating equation (4) over the frequency yields

$$\left\langle I^2 \right\rangle = \int_0^\infty S_I(\omega)\frac{d\omega}{2\pi} = \frac{k_BT}{L_K}. \tag{5}$$

In other words, in the classical regime, the current noise follows the equipartition theorem, storing a mean thermal energy of $k_BT/2$ into the collective degree of freedom associated with L_K.

So, in principle the collective inertial effect L_K influences the thermal noise spectrum. But little attention has been paid to this effect, as it is not too conspicuous—if not negligible—in most traditional conductors. To see this, note that the Planck factor in equation (1) rolls off with frequency with a characteristic cutoff $\omega_q \equiv k_BT/\hbar$, while $\Re\{Y(\omega)\}$ rolls off with a characteristic cutoff $\omega_p \equiv R/L_K = \tau^{-1}$ (τ: electron momentum relaxation time), where $R/L_K = \tau^{-1}$ is from the semiclassical calculation of the ac conductivity [6]. In traditional conductors, ω_q tends to be smaller than, or at best comparable to, ω_p across a broad temperature range, rendering the L_K effect masked in the spectrum. But in recently advanced nanoscale or low-dimensional conductors such as graphene, τ is large enough that $\omega_p \ll \omega_q$ is possible [8, 9], in which case the L_K effect will dominate the spectrum roll-off.

The purpose of this paper is to highlight this collective inertial effect on the thermal noise spectrum from both fundamental microscopic and practical modeling points of view. In section 2, we will delineate the effect from a microscopic standpoint. The collective excitation of electrons, macroscopically represented by L_K, exhibits a well-defined collective mass [5, 8, 10]. Since its acceleration is essential for propagating the plasmonic wave [5, 8, 11–15], we will call this collective mass, normalized to the number of electrons, as the plasmonic mass m_p. We will elucidate that the correct mass to use in describing the microscopic dynamics of thermal fluctuation is not the single-electron effective mass m^* but the plasmonic mass m_p. In fact, this essential link between m_p (or L_K) and thermal noise is subsumed by, and thus a natural consequence of, the linear response theory; i.e., both the fluctuation-dissipation theorem and m_p are attained from the same linear response framework applied to the collection of electrons [3, 4]. In section 3, we will elaborate on how the plasmonic roll-off can take over the Planck (quantum) roll-off in the noise spectrum for large enough τ. Section 4 will use graphene as an example conductor and develop its thermal noise model, considering the plasmonic mass effect from both electron and hole bands that co-exist.

2. Collective mode and noise: microscopic view

2.1. Plasmonic mass

We first detail the concept of plasmonic mass [8] that is paramount in this paper. If we collectively displace each electron in a conductor—e.g., by applying an electric field and setting a current—by δ in the k_x direction, the total energy of the electron system is increased. The *increase amount* is the collective kinetic energy E_K corresponding to the current; it is given by

$$E_K = Wl\int\frac{d^d\mathbf{k}}{(2\pi)^d}g\epsilon\left(\mathbf{k} + \delta\hat{\mathbf{k}}_x\right)f(\epsilon(\mathbf{k})) - Wl\int\frac{d^d\mathbf{k}}{(2\pi)^d}g\epsilon(\mathbf{k})f(\epsilon(\mathbf{k})), \tag{6}$$

where the integration is over the conduction band—up to section 3, we focus on a conductor with a single conduction band—and $\hat{\mathbf{k}}_x$ is a unit vector along the k_x axis. For a small enough δ, which is practically always the case, we can write equation (6) in powers of δ

$$E_K = \delta \times Wlg\int\frac{d^d\mathbf{k}}{(2\pi)^d}\frac{\partial\epsilon}{\partial k_x}f(\epsilon(\mathbf{k})) + \frac{\delta^2}{2}\times Wlg\int\frac{d^d\mathbf{k}}{(2\pi)^d}\frac{\partial^2\epsilon}{\partial k_x^2}f(\epsilon(\mathbf{k})) + \ldots \tag{7}$$

If we assume inversion symmetry $\epsilon(\mathbf{k}) = \epsilon(-\mathbf{k})$, met by many lattice types, the first term vanishes. But more broadly, since the first term is proportional to the integration of the group velocity, $v_x(\mathbf{k}) = (1/\hbar)(\partial\epsilon/\partial k_x)$, weighted by the Fermi–Dirac distribution, if it did not vanish, there would be a spontaneous current; we do not consider such a case here, and set the first term to zero. Now, as δ and the collective crystal momentum P are related by $P = nWl \times \hbar\delta$ —here, $n = \int (\mathrm{d}^d\mathbf{k}/(2\pi)^d) g f(\epsilon(\mathbf{k}))$ is electron number density per area or volume ($d = 2$ or 3)— equation (7) becomes

$$E_\mathrm{K} = \frac{P^2}{2} \times \frac{g}{\hbar^2 n^2 Wl} \int \frac{\mathrm{d}^d\mathbf{k}}{(2\pi)^d} \frac{\partial^2\epsilon}{\partial k_x^2} f(\epsilon(\mathbf{k})). \tag{8}$$

So $E_\mathrm{K} \propto \delta^2 \propto P^2$ regardless of $\epsilon(\mathbf{k})$. This quadratic relation is expected, as E_K is minimum at $\delta = 0$ (whether the electrons move to the right or left, E_K increases). As $E_\mathrm{K} \propto P^2$ is Newtonian, the collective inertia is

$$M = \frac{P^2}{2E_\mathrm{K}} = \frac{\hbar^2 n^2 Wl}{g} \left[\int \frac{\mathrm{d}^d\mathbf{k}}{(2\pi)^d} \frac{\partial^2\epsilon}{\partial k_x^2} f(\epsilon(\mathbf{k})) \right]^{-1}. \tag{9}$$

Collective mass per electron—plasmonic mass—is then

$$m_\mathrm{p} = \frac{\hbar^2 n}{g} \left[\int \frac{\mathrm{d}^d\mathbf{k}}{(2\pi)^d} \frac{\partial^2\epsilon}{\partial k_x^2} f(\epsilon(\mathbf{k})) \right]^{-1} \tag{10}$$

which is the harmonic mean of the effective mass tensor component $\hbar^2[\mathbf{M}^{-1}(\mathbf{k})]_{xx} = \partial^2\epsilon/\partial k_x^2$. For later use, we re-express equation (10) after integration by parts:

$$m_\mathrm{p} = \frac{n}{g} \left[\int \frac{\mathrm{d}^d\mathbf{k}}{(2\pi)^d} v_x^2(\mathbf{k}) \left(-\frac{\partial f}{\partial\epsilon} \right) \right]^{-1}. \tag{11}$$

We now make a few key observations about m_p.

(1) *Plasmonic mass versus effective mass:* For a general $\epsilon(\mathbf{k})$, m_p differs from the single-electron effective mass, $m^* = [1/\hbar^2 \times \partial^2\epsilon(\mathbf{k})/\partial k_x^2]^{-1}$. m_p is $\mathbf{k}$-independent, while m^* is generally $\mathbf{k}$-dependent. m_p generally varies with T and n, for it arises from the collective excitation, while m^* does not. In the special case of $\epsilon(\mathbf{k}) \propto k^2$ ($k \equiv |\mathbf{k}|$), m^* is a well-defined, $\mathbf{k}$-independent constant, and $m^* = m_\mathrm{p}$, as seen from equation (10) in connection with $n = \int (\mathrm{d}^d\mathbf{k}/(2\pi)^d) g f(\epsilon(\mathbf{k}))$.

(2) *Plasmonic mass versus cyclotron mass:* Consider a 2D conductor at $T = 0$ with an isotropic single-electron dispersion, $\epsilon(\mathbf{k}) = \epsilon(k)$. Integrations in equation (10) and $n = \int (\mathrm{d}^2\mathbf{k}/4\pi^2) g f(\epsilon(\mathbf{k}))$ for $|\mathbf{k}| \leqslant k_\mathrm{F}$ yield $m_\mathrm{p}(T = 0) = \hbar^2 k_\mathrm{F} (\mathrm{d}k/\mathrm{d}\epsilon)_{k=k_\mathrm{F}}$ (k_F: Fermi wavenumber). On the other hand, the cyclotron mass for electrons that orbit around the Fermi surface enclosing the $\mathbf{k}$-space area of $A(\epsilon)$ is $m_\mathrm{c} = \hbar^2/(2\pi)[(\mathrm{d}/\mathrm{d}\epsilon)A(\epsilon)]_{\epsilon=\epsilon_\mathrm{F}}$ [6, 16], which, for isotropic 2D conductors, is

$$m_\mathrm{c} = \frac{\hbar^2}{2\pi} \left[\frac{\mathrm{d}k}{\mathrm{d}\epsilon} \cdot \frac{\mathrm{d}\left(\pi k^2\right)}{\mathrm{d}k} \right]_{k=k_\mathrm{F}} = \hbar^2 k_\mathrm{F} \left(\frac{\mathrm{d}k}{\mathrm{d}\epsilon} \right)_{k=k_\mathrm{F}}. \tag{12}$$

Thus, for a 2D isotropic conductor, $m_\mathrm{p}(T = 0) = m_\mathrm{c}$. This also applies to three-dimensional (3D) conductors with $\epsilon(\mathbf{k}) = \epsilon(k)$.

(3) *Graphene:* While the single-electron energy dispersion $\epsilon(\mathbf{k})$ for graphene is that of massless Dirac Fermions, $m_\mathrm{p} \neq 0$. As graphene is isotropic with $\epsilon(\mathbf{k}) = \hbar v_\mathrm{F} k$, $m_\mathrm{p}(T = 0) = m_\mathrm{c} = \epsilon_\mathrm{F}/v_\mathrm{F}^2$, like the rest mass in relativity (ϵ_F and v_F are Fermi energy and velocity). m_c was measured from Shubnikov–de Haas oscillations [17, 18]. m_p was hinted at from the measured plasmonic dispersion [19, 20] and was recently directly measured by accelerating it with a microwave field [8].

(4) *Plasmonic mass versus kinetic inductance:* The current due to the collective shift of electrons is an integral over the *perturbed* group velocity, $v_x(\mathbf{k} + \delta\hat{\mathbf{k}}_x)$:

$$I = W \int \frac{\mathrm{d}^d\mathbf{k}}{(2\pi)^d} g e v_x\left(\mathbf{k} + \delta\hat{\mathbf{k}}_x\right) f(\epsilon(\mathbf{k})), \tag{13}$$

which, to the first order of δ, is

$$I = \delta \times \frac{Wge}{\hbar} \int \frac{\mathrm{d}^d\mathbf{k}}{(2\pi)^d} \frac{\partial^2\epsilon}{\partial k_x^2} f(\epsilon(\mathbf{k})). \tag{14}$$

Thus $E_\mathrm{K} \propto \delta^2 \propto I^2$, and we identify the constant of proportionality as $L_\mathrm{K}/2 = E_\mathrm{K}/I^2$. Using equations (8) and (14), we have:

$$L_\mathrm{K} = \frac{l}{W} \frac{\hbar^2}{ge^2} \left[\int \frac{\mathrm{d}^d\mathbf{k}}{(2\pi)^d} \frac{\partial^2\epsilon}{\partial k_x^2} f(\epsilon(\mathbf{k})) \right]^{-1}. \tag{15}$$

This is identical to equation (2) obtained from the semiclassical calculation of the ac conductivity [6]. Finally, from equations (10) and (15), we obtain

$$L_\mathrm{K} = \frac{l}{W} \frac{m_\mathrm{p}}{ne^2}. \tag{16}$$

This establishes the link between macroscopic L_K and microscopic m_p. Equation (16) is the generalization of the more familiar expression for L_K derived from the Drude model for the special case of $\epsilon(\mathbf{k}) \propto k^2$ and $m_\mathrm{p} = m^*$.

2.2. From macroscopic to microscopic picture

In the introduction, we established the macroscopic energy equipartition in the classical regime, equation (5); the noise current I stores a thermal energy of $k_\mathrm{B}T/2$ into L_K. We now convert this macroscopic energy equipartition to a microscopic form applicable to the thermal fluctuation velocity v_fl —along the x-axis where noise is measured—for an individual electron. As each electron contributes a fluctuating current of $v_\mathrm{fl}e/l$, $\langle I^2\rangle = \langle v_\mathrm{fl}^2\rangle \mathrm{e}^2/l^2 \times nWl$. By combining this with equations (5) and (16), we obtain

$$\langle v_\mathrm{fl}^2\rangle = \frac{k_\mathrm{B}T}{m_\mathrm{p}}, \tag{17}$$

which holds for arbitrary $\epsilon(\mathbf{k})$. While the thermal motions of electrons are not apparently collective, the fluctuating velocity stores a thermal energy of $k_\mathrm{B}T/2$ into the plasmonic mass m_p —as opposed to the single-electron effective mass m^*—with the plasmonic motion being an appropriate degree of freedom

to apply the energy equipartition at the microscopic level. We emphasize that the energy equipartition does not apply generally to m^*, i.e., $\left\langle v_{\rm fl}^2 \right\rangle \neq k_{\rm B}T/m^*$, in general. While $\left\langle v_{\rm fl}^2 \right\rangle = k_{\rm B}T/m^*$ is valid when $\epsilon(\mathbf{k}) \propto k^2$ and $m^* = m_{\rm p}$, it faces a problem for a general, non-parabolic $\epsilon(\mathbf{k})$, where m^* is dependent on $\mathbf{k}$. A more dramatic example where $\left\langle v_{\rm fl}^2 \right\rangle = k_{\rm B}T/m^*$ fails is the case of graphene, where individual electrons act as massless Dirac Fermions. In sum, the proper mass to use in describing thermal noise dynamics is not m^* but $m_{\rm p}$. In the time-domain description, the Langevin equation [3] should use $m_{\rm p}$, not m^*.

2.3. From microscopic to macroscopic picture

The foregoing discussion started by integrating the power spectral density of equation (4) into the macroscopic equipartition of equation (5) and subsequently obtained the microscopic equipartition of equation (17). We may reverse this chain of processes, and derive first the microscopic equipartition by enumerating and averaging the effect of each individual electron, based on the Fermi–Dirac statistics.

To this end, for a $\mathbf{k}$-state, we define a unitless random variable $s_{\mathbf{k}}$, which assumes a value of 1 with probability $f(\epsilon(\mathbf{k}))$ and a value of 0 with probability $1 - f(\epsilon(\mathbf{k}))$. That is, $s_{\mathbf{k}} = 1$ means that the $\mathbf{k}$-state is occupied by an electron, while $s_{\mathbf{k}} = 0$ signifies the emptiness of the $\mathbf{k}$-state. Then, the sum of the x-component group velocities of all electrons in the conductor can be written as

$$v_{\rm sum} = \sum_{\mathbf{k}} v_x(\mathbf{k}) s_{\mathbf{k}}, \tag{18}$$

which itself is a random variable. Its variance, which represents the fluctuation in the velocity sum, must be related to the above-discussed $\langle v_{\rm fl}^2 \rangle$ by:

$$nWl \times \langle v_{\rm fl}^2 \rangle = \langle v_{\rm sum}^2 \rangle - \langle v_{\rm sum} \rangle^2. \tag{19}$$

We evaluate each term on the right-hand side by using equation (18). The first term is

$$\begin{aligned} \langle v_{\rm sum}^2 \rangle &= \left\langle \left(\sum_{\mathbf{k}} v_x(\mathbf{k}) s_{\mathbf{k}} \right)^2 \right\rangle \\ &= \sum_{\mathbf{k}} v_x^2(\mathbf{k}) \langle s_{\mathbf{k}}^2 \rangle + \sum_{\mathbf{k} \neq \mathbf{k}'} v_x(\mathbf{k}) v_x(\mathbf{k}') \langle s_{\mathbf{k}} s_{\mathbf{k}'} \rangle \\ &= \sum_{\mathbf{k}} v_x^2(\mathbf{k}) f_{\mathbf{k}} + \sum_{\mathbf{k} \neq \mathbf{k}'} v_x(\mathbf{k}) v_x(\mathbf{k}') f_{\mathbf{k}} f_{\mathbf{k}'}, \end{aligned}$$

where $f_{\mathbf{k}}$ is a shorthand notation for $f(\epsilon(\mathbf{k}))$, and we have used $\langle s_{\mathbf{k}} s_{\mathbf{k}'} \rangle = \langle s_{\mathbf{k}} \rangle \langle s_{\mathbf{k}'} \rangle$ for $\mathbf{k} \neq \mathbf{k}'$, $\langle s_{\mathbf{k}} \rangle = 1 \cdot f_{\mathbf{k}} + 0 \cdot (1 - f_{\mathbf{k}}) = f_{\mathbf{k}}$, and $\langle s_{\mathbf{k}}^2 \rangle = 1^2 \cdot f_{\mathbf{k}} + 0^2 \cdot (1 - f_{\mathbf{k}}) = f_{\mathbf{k}}$. Similarly,

$$\begin{aligned} \langle v_{\rm sum} \rangle^2 &= \left(\sum_{\mathbf{k}} v_x(\mathbf{k}) \langle s_{\mathbf{k}} \rangle \right)^2 \\ &= \sum_{\mathbf{k}} v_x^2(\mathbf{k}) f_{\mathbf{k}}^2 + \sum_{\mathbf{k} \neq \mathbf{k}'} v_x(\mathbf{k}) v_x(\mathbf{k}') f_{\mathbf{k}} f_{\mathbf{k}'}. \end{aligned}$$

By plugging these two results into equation (19), we obtain

$$\langle v_{\rm fl}^2 \rangle = \frac{1}{nWl} \sum_{\mathbf{k}} v_x^2(\mathbf{k}) f_{\mathbf{k}} \left(1 - f_{\mathbf{k}} \right). \tag{20}$$

In the special case where there is inversion symmetry in the single-electron energy dispersion, i.e., $\epsilon(\mathbf{k}) = \epsilon(-\mathbf{k})$ and $v_x(\mathbf{k}) = -v_x(-\mathbf{k})$, equation (20) has a particularly simple interpretation. In this case, if a $\mathbf{k}$-state and a $-\mathbf{k}$-state are both occupied, the group velocities of the two occupant electrons cancel each other due to the symmetry, not contributing to the fluctuation. Thus to evaluate $\langle v_{\rm fl}^2 \rangle$ in this special case, one has to enumerate only those situations where the $\mathbf{k}$-state is occupied while the $-\mathbf{k}$-state is not. The corresponding probability is then $f_{\mathbf{k}} \left(1 - f_{-\mathbf{k}} \right) = f_{\mathbf{k}} \left(1 - f_{\mathbf{k}} \right)$, and hence equation (20). However, in attaining equation (20), we have not imposed any condition on $\epsilon(\mathbf{k})$—such as the inversion symmetry— and, hence, equation (20) is generally valid.

Converting equation (20) into an integral and using $f(\epsilon(\mathbf{k}))[1 - f(\epsilon(\mathbf{k}))] = -k_{\rm B}T(\partial f/\partial \epsilon)$, we obtain

$$\begin{aligned} \langle v_{\rm fl}^2 \rangle &= \frac{1}{n} \int \frac{{\rm d}^d \mathbf{k}}{(2\pi)^d} g v_x^2(\mathbf{k}) f(\epsilon(\mathbf{k}))[1 - f(\epsilon(-\mathbf{k}))] \\ &= \frac{g k_{\rm B} T}{n} \int \frac{{\rm d}^d \mathbf{k}}{(2\pi)^d} v_x^2(\mathbf{k}) \left(-\frac{\partial f}{\partial \epsilon} \right) \\ &= \frac{k_{\rm B}T}{m_{\rm p}}, \end{aligned} \tag{21}$$

where we have taken the last step by using equation (11). As seen, the microscopic equipartition with $m_{\rm p}$ resurfaces but this time via the *ab initio* calculation, which reaffirms the critical relevance of $m_{\rm p}$ to noise dynamics.

Equation (16) with $\langle I^2 \rangle = \langle v_{\rm fl}^2 \rangle {\rm e}^2/l^2 \times nWl$ transforms this microscopic equipartition into the macroscopic equipartition, equation (5). We can subsequently work out the noise power spectral density: As $\langle I(0)I(t) \rangle = \langle I^2 \rangle {\rm e}^{-|t|/\tau}$ [3], $S_I(\omega) = 4 \int_0^\infty {\rm d}t \langle I(0)I(t) \rangle \cos(\omega t) = 4\langle I^2 \rangle \tau/(1 + \omega^2 \tau^2)$; by using equation (5) and $\tau = L_{\rm K}/R$, we obtain the noise power spectral density of equation (4).

The power spectral density derivation above tacitly assumed frequency-independent τ and R. But even when τ and R are frequency-dependent, we can still derive the power spectral density from the microscopic equipartition $\langle v_{\rm fl}^2 \rangle = k_{\rm B}T/m_{\rm p}$ by using the generalized Langevin equation of Kubo's linear response theory [3], where (and importantly) $m_{\rm p}$ is to be used instead of m^*.

3. High-frequency behavior of $S_I(\omega)$

With $Y(\omega) = (R + i\omega L_{\rm K})^{-1}$, equation (1) is written out as

$$S_I(\omega) = 4k_{\rm B}T \cdot \frac{R}{R^2 + \omega^2 L_{\rm K}^2} \cdot \frac{\hbar\omega/k_{\rm B}T}{\exp\left(\hbar\omega/k_{\rm B}T\right) - 1}. \tag{22}$$

The second factor is $\Re\{Y(\omega)\}$, and the third Planck factor is due to the radiation quantization. With frequency, the Planck

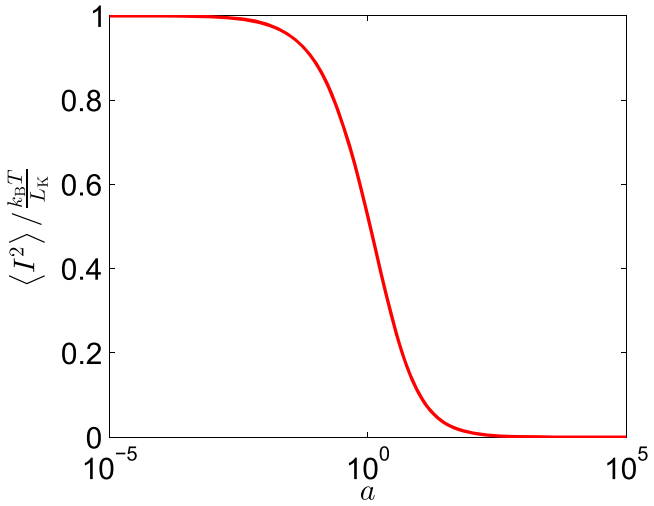

Figure 2. $\langle I^2 \rangle$ normalized to $k_B T/L_K$ versus $a \equiv \omega_p/\omega_q$.

factor starts rolling off at around the 'quantum cutoff,' $\omega_q = k_B T/\hbar$; at $T = 300$ K, $\omega_q/(2\pi) \sim 6.25$ THz. On the other hand, $\Re\{Y(\omega)\}$ starts rolling off at around the 'plasmonic cutoff,' $\omega_p = R/L_K = 1/\tau$. In most typical conductors with τ between $\sim 10^{-14}$ s and $\sim 10^{-16}$ s, ω_p tends to be larger than, or, at best, comparable to, ω_q. So the noise spectrum roll-off due to L_K (or m_p) is typically masked (or, at best, blurred) by that due to the Planck factor.

By contrast, recent advances in nanoscale or low-dimensional conductors such as graphene have greatly increased τ so that $\omega_p \ll \omega_q$ is possible [8, 9], with which $Y(\omega)$ becomes substantially inductive at GHz to THz frequencies and the spectrum roll-off due to L_K kicks in before the Planck factor suppresses the spectrum. To show this concretely, figure 1(b) plots equation (22)—noise spectrum versus frequency—for various values of τ. For $\tau = 0$ (black curve), the noise spectrum starts decreasing at around ω_q; this is the noise suppression due purely to the Planck factor. As τ is increased and ω_p becomes increasingly smaller than ω_q, the high-frequency suppression of the noise spectrum becomes increasingly dominated by the L_K effect; compare the blue, green, and red curves—τ increasing in that order—against the black curve. For such large τ values, the L_K effect on thermal noise is critical to model in. This effect may also be exploited to infer the optical (plasmonic) properties from the noise spectrum.

To further highlight the critical role of L_K in the noise spectrum for large τ, we compute $\langle I^2 \rangle$ by integrating equation (22) across the entire frequency:

$$\left\langle I^2 \right\rangle = \frac{k_B T}{L_k} \times \frac{2}{\pi} \int_0^\infty \frac{a}{a^2 + x^2} \frac{x \mathrm{d}x}{\mathrm{e}^x - 1} \tag{23}$$

where $a \equiv \omega_p/\omega_q = R\hbar/(k_B T L_K) = \hbar/(k_B T \tau)$ and $x \equiv \hbar\omega/(k_B T)$. This generalizes equation (5) by including the Planck quantization. $\langle I^2 \rangle$ versus a is in figure 2. For $a \to \infty$ ($\tau \to 0$; $\omega_p \gg \omega_q$), the Planck quantization effect takes precedence over the L_K effect, and $\langle I^2 \rangle \ll k_B T/L_K$. In fact, in this case, equation (23) is reduced to

$$\left\langle I^2 \right\rangle = \frac{k_B T}{L_K} \times \frac{2}{\pi a} \int_0^\infty \frac{x \mathrm{d}x}{\mathrm{e}^x - 1} = \frac{\pi (k_B T)^2}{3R\hbar} \tag{24}$$

where L_K disappears. In contrast, for $a \to 0$ ($\tau \to \infty$; $\omega_p \ll \omega_q$), we have

$$\left\langle I^2 \right\rangle = \frac{k_B T}{L_K} \times \frac{2a}{\pi} \int_0^\infty \frac{1}{a^2 + x^2} \mathrm{d}x = \frac{k_B T}{L_K}, \tag{25}$$

recovering the macroscopic equipartition, equation (5); i.e., in this case, the spectrum roll-off is entirely governed by L_K, with the Planck quantization effect masked.

4. Thermal noise model for graphene

Graphene is an ideal system to apply the foregoing formalism to and to derive a thermal noise model from for a few reasons. First, in high-quality graphene, $\tau \sim 10^{-12}$ s [8, 9], corresponding to the green curve of figure 1(b), and, hence, the effect of L_K (or m_p) dominates over the Planck quantization effect in the noise spectrum. Second, in graphene, individual electrons act as massless Dirac Fermions, yet $m_p \neq 0$, and, hence, m_p varies with n and T, enriching the noise behaviors (in contrast, in conductors with $\epsilon(\mathbf{k}) \propto k^2$ and $m_p = m^* \neq 0$, m_p is independent of n and T). Third, since in graphene both conduction and valence bands contribute to electronic conduction, L_K (or m_p) from both bands should be considered, which further complicates the noise behaviors.

First consider a fictitious graphene with only a conduction band, held at a constant charge density by a gate bias. With only the electron band, the constant charge density means a constant electron number density n. Suppose $\mu(T = 0) = \epsilon_F = 0.1$ eV. With $g = 4$, $n = \int (\mathrm{d}^2\mathbf{k}/\pi^2) f(\epsilon(\mathbf{k}))|_{\mu=\epsilon_F, T=0} = \epsilon_F^2/(\pi\hbar^2 v_F^2)$. As n is T-independent in our scenario,

$$n = \int \frac{\mathrm{d}^2\mathbf{k}}{\pi^2} f(\epsilon(\mathbf{k}))|_{\mu,T} = \frac{1}{\pi} \frac{\epsilon_F^2}{\hbar^2 v_F^2}, \tag{26}$$

from which $\mu(T)$ is determined (figure 3(a), blue curve). Using this $\mu(T)$ in equation (10), we evaluate m_p. As n is constant, $L_K \propto m_p$ (equation (16)). Figure 3(b) shows L_K and m_p as functions of T; both increase with T. This contrasts the case of a conventional conductor with parabolic dispersion, for which m_p (and L_K with the fixed n with the gate biasing) is independent of T.

A real graphene sample where electron and hole bands co-exist exhibits even richer behaviors. We again assume a constant charge density held by a gate bias and suppose $\mu(T = 0) = \epsilon_F = 0.1$ eV. At $T = 0$, graphene is electron-doped. As T rises, both the electron number density n_e and hole number density n_h—subscript 'e' and 'h' signify electron and hole bands—can vary (this contrasts the fictitious case where the electron number density is fixed) while the total

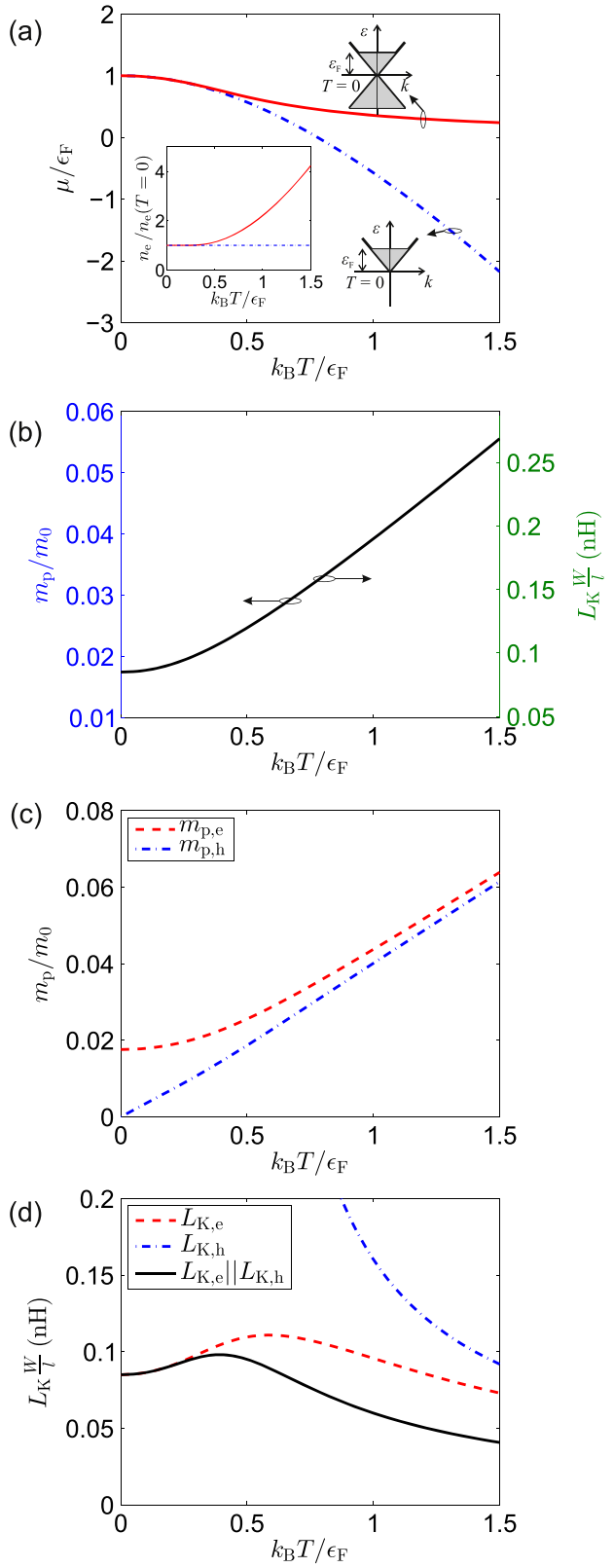

Figure 3. (a) $\mu(T)$ for fictitious graphene (blue curve) and real graphene (red curve), shown with electronic band structures. $\epsilon_F = 0.1$ eV for both. Inset: n_e for both systems. (b). m_p, L_K versus T for fictitious graphene. m_0 is intrinsic electron mass. (c) m_p in each band versus T for real graphene. (d) L_K in each band versus T for real graphene. $L_{K,e}||L_{K,h}$ is also shown.

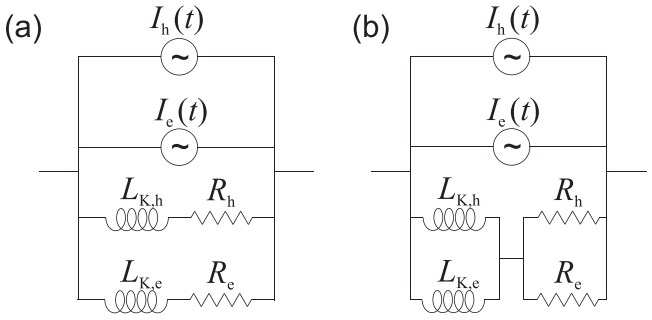

Figure 4. (a) Circuit noise model for graphene. (b) For $\tau_e = \tau_h$.

charge density $-en_e + en_h$ is fixed. Formally:

$$n_e(\mu, T) - n_h(\mu, T) = \frac{1}{\pi}\frac{\epsilon_F^2}{\hbar^2 v_F^2}, \tag{27}$$

where

$$n_e(\mu, T) = \int_e \frac{d^2\mathbf{k}}{\pi^2} f(\epsilon(\mathbf{k}))|_{\mu,T}, \tag{28}$$

$$n_h(\mu, T) = \int_h \frac{d^2\mathbf{k}}{\pi^2}\Big[1 - f(\epsilon(\mathbf{k}))|_{\mu,T}\Big]. \tag{29}$$

This leads to a markedly different behavior for $\mu(T)$, with $\mu \to 0$ for $T \to \infty$ (figure 3(a), red curve), as compared to the case of the fictitious graphene (figure 3(a), blue curve). Once $\mu(T)$ is evaluated, $n_e(T)$ and $n_h(T)$ follow from equations (28) and (29). Also with $\mu(T)$, we can evaluate $m_{p,e}$ and $m_{p,e}$,

$$m_{p,e} = \frac{\hbar^2 n_e}{g}\left[\int_e \frac{d^d\mathbf{k}}{(2\pi)^d}\frac{\partial^2\epsilon}{\partial k_x^2} f(\epsilon(\mathbf{k}))|_{\mu,T}\right]^{-1}, \tag{30}$$

$$m_{p,h} = \frac{\hbar^2 n_h}{g}\left[\int_h \frac{d^d\mathbf{k}}{(2\pi)^d}\frac{\partial^2\epsilon}{\partial k_x^2}\Big[1 - f(\epsilon(\mathbf{k}))|_{\mu,T}\Big]\right]^{-1}, \tag{31}$$

which are variations of equation (10). Finally, using the results above in equation (16), we can compute the kinetic inductance L_K of each band separately.

Figures 3(c) and (d) plot the resulting m_p and L_K in each band as functions of T. They again exhibit conspicuous T dependency, just like in the fictitious case. However, the T-dependency of $L_{K,e}$ with a maximum value (figure 3(d)) markedly differs from the monotonically increasing T-dependency of $L_{K,e}$ in the fictitious case (figure 3(b)). $L_{K,e} \sim m_{p,e}/n_e$ (equation (16)) exhibits the maximum value in the real graphene due to competing effects of $m_{p,e}$ and n_e. For small T, $n_h \ll n_e \approx$ constant, so $L_{K,e}$ increases with T as $m_{p,e}$ increases with T. This is just like in the fictitious case. In contrast, for large T, n_e grows as T^2 (as does n_h to keep the overall charge density constant), which is faster than the growth of $m_{p,e}$ with T (compare figure 3(a) inset and figure 3(c)); therefore, $L_{K,e} \sim m_{p,e}/n_e$ decreases for large T.

The circuit noise model of the real graphene is shown in figure 4(a), where the L_K effects from both bands is explicitly modeled in. The total power spectral density of the current

noise is given by

$$S_I(\omega) = 4k_B T\left[\frac{R_e}{R_e^2 + \omega^2 L_{K,e}^2} + \frac{R_h}{R_h^2 + \omega^2 L_{K,h}^2}\right] \times \frac{\hbar\omega/k_B T}{\exp\left(\hbar\omega/k_B T\right) - 1} \quad (32)$$

assuming no correlation between the electron band noise and hole band noise. Due to the dominance of $L_{K,e}$ and $L_{K,h}$ in the spectrum roll-off over the Planck quantization effect (in high-quality graphene) and due also to the rich T-dependencies of $L_{K,e}$ and $L_{K,h}$, the noise power spectral density in graphene exhibits very different characteristics from that in traditional conductors in terms of both frequency and temperature dependency. Whether the electron and hole band noise are correlated or not is an open question; such correlation, if extant and conspicuous, would further enrich the noise spectrum. Also note that we have ignored inter-band transitions, because they are minimal at our frequencies of interest (up to THz) for this relatively highly doped sample.

If τ is the same for both bands, i.e., if $L_{K,e}/R_e = L_{K,h}/R_h$, equation (32) is reduced to

$$S_I(\omega) = 4k_B T\frac{R_e||R_h}{\left(R_e||R_h\right)^2 + \omega^2\left(L_{K,e}||L_{K,h}\right)^2} \times \frac{\hbar\omega/k_B T}{\exp\left(\hbar\omega/k_B T\right) - 1} \quad (33)$$

where $(R_e||R_h)^{-1} = R_e^{-1} + R_h^{-1}$ and $(L_{K,e}||L_{K,h})^{-1} = L_{K,e}^{-1} + L_{K,h}^{-1}$. That is, the circuit model of figure 4(a) can be reduced to figure 4(b), with the resistors from both bands and the kinetic inductors from both bands each connected in parallel, with $R_e||R_h$ and $L_{K,e}||L_{K,h}$ in series serving as overall resistor and inductor. For the T-dependency of $L_{K,e}||L_{K,h}$, see figure 3(d).

In general, $L_{K,e}/R_e \neq L_{K,h}/R_h$, but even in such a case, $L_{K,e}||L_{K,h}$ considered right above is still of great relevance to the noise dynamics. This is because $\langle I^2\rangle = \langle I_e^2\rangle + \langle I_h^2\rangle = k_B T/L_{K,e} + k_B T/L_{K,h}$, or,

$$\langle I^2\rangle = \frac{k_B T}{L_{K,e}||L_{K,h}}. \quad (34)$$

That is, the total integrated current noise fluctuation follows the energy equipartition, with the mean thermal energy of $k_B T/2$ stored onto the macroscopic degree of freedom associated with $L_{K,e}||L_{K,h}$. Since this parallel inductance exhibits the T dependency, as shown in figure 3(d), $\langle I^2\rangle$ in graphene is no longer proportional to T, which is the case for conductors with quadratic single-electron energy dispersion held with a gate bias.

Two additional points on the graphene thermal noise model of figure 4(a) may merit mentioning.

Parasitic effects: Since in graphene the magnetic inductance is two or more orders of magnitude smaller than the kinetic inductance [8], it was ignored in the noise model of figure 4(a). The model does not explicitly show the shunt parasitic capacitance (consisting of classical and quantum capacitance in series in general) to ground—the ground can be provided by a proximate conducting gate, or is defined as the reference potential at an infinitely far point in the absence of gate [8]—because the shunt capacitance does not affect the expression of the intrinsic noise current.

Lumped versus distributed model: figure 4(a) is a lumped circuit model. In the case where the graphene strip is long enough to be comparable to, or larger than, the plasmonic wavelength, the graphene strip can be modeled as a plasmonic transmission line consisting of an infinite number of distributed infinitesimal segments, with each segment appearing like figure 4(a) with the aforementioned shunt capacitance (to ground) added; here the inductance, resistance, capacitance, and current noise of each segment has to be scaled to its infinitesimal length [8]. The noise spectrum at either terminal of this transmission line then can be evaluated from the noise sources distributed along the lossy plasmonic transmission line [21].

5. Conclusion

Recent advances in low-dimensional materials have blurred the traditional boundary between photonics and electronics. A prominent example is plasmonics in 2D conductors (e.g., graphene); while plasmonic excitation occurs traditionally in the realm of photonics, in 2D materials it can occur at THz and GHz frequencies, reaching into the electronics realm.

This paper offered another example that highlights such a merger of photonics–electronics boundaries. Concretely, we investigated how the plasmonic response (traditionally studied in photonics) can significantly alter the Johnson–Nyquist thermal noise dynamics (traditionally studied in electronics). The intrinsic connection between plasmonics and Johnson–Nyquist noise is in fact a natural consequence of the linear response theory: that is, both plasmonic properties and the fluctuation-dissipation relation (of which the Johnson–Nyquist noise is a prominent example) are obtained from the same linear response framework applied to the collection of electrons. But in traditional conductors with short electron scattering times, the Planck quantization effect has masked the plasmonic effect in the noise spectrum. On the other hand, in 2D materials like graphene, where the electron scattering time has been greatly elongated, the plasmonic effect can take precedence over the Planck quantization effect, significantly altering the thermal noise spectrum. We demonstrated that this effect is not only of great importance for practical noise modeling, but it also provides an opportunity to delineate some fundamental concepts, in particular, the critical role that the plasmonic mass (as opposed to the single-electron effective mass) plays in thermal fluctuation dynamics of electrons.

To emphasize the practical relevance of this study, the last section of this paper was dedicated to developing the thermal noise model for graphene, where individual electrons act as massless Dirac Fermions, while the plasmonic mass is non-zero. We demonstrated that in graphene, due to the dominance of the plasmonic mass effect over the Planck quantization effect, the temperature dependence of the

plasmonic mass, and the emergence of the plasmonic mass from both electron and hole bands that co-exist, the thermal noise spectrum shows rich temperature and frequency dependency, unprecedented in traditional conductors.

Acknowledgments

The authors thank Prof Philip Kim, Prof Bert Halperin, and Dr Kitty Y M Yeung of Harvard University for their valuable discussions. We acknowledge the support by the Air Force Office of Scientific Research under contract FA9550–13-1–0211, the Office of Naval Research under contract N00014–13-1–0806, and the National Science Foundation STC Center for Integrated Quantum Materials under contract DMR-1231319. Jingyee Chee acknowledges financial support from the National Science Scholarship, Singapore.

References

[1] Johnson J B 1928 Thermal agitation of electricity in conductors *Phys. Rev.* **32** 97–109
[2] Nyquist H 1928 Thermal agitation of electric charge in conductors *Phys. Rev.* **32** 110–3
[3] Kubo R 1966 The fluctuation-dissipation theorem *Rep. Prog. Phys.* **29** 255
[4] Callen H and Welton T 1951 Irreversibility and generalized noise *Phys. Rev.* **83** 34–40
[5] Yoon H, Yeung K Y M, Kim P and Ham D 2014 Plasmonics with two-dimensional conductors *Phil. Trans. R. Soc.* A **372** 20130104
[6] Ashcroft N W and Mermin N D 1976 *Solid State Physics* 1st edn (New York: Cengage Learning)
[7] Ehrenreich H and Cohen M H 1959 Self-consistent field approach to the many-electron problem *Phys. Rev.* **115** 786–90
[8] Yoon H, Forsythe C, Wang L, Tombros N, Watanabe K, Taniguchi T, Hone J, Kim P and Ham D 2014 Measurement of collective dynamical mass of dirac fermions in graphene *Nat. Nanotechnology* **9** 594–99
[9] Dean C R *et al* 2010 Boron nitride substrates for high-quality graphene electronics *Nat. Nanotechnology* **5** 722–26
[10] Abedinpour S H, Vignale G, Principi A, Polini M, Tse W K and MacDonald A H 2011 Drude weight, plasmon dispersion, and ac conductivity in doped graphene sheets *Phys. Rev.* B **84** 045429
[11] Yan H, Xia F, Li Z and Avouris P 2012 Plasmonics of coupled graphene micro-structures *New J. Phys.* **14** 125001
[12] Yan H, Li X, Chandra B, Tulevski G, Wu Y, Freitag M, Zhu W, Avouris P and Xia F 2012 Tunable infrared plasmonic devices using graphene/insulator stacks *Nat. Nanotechnology* **7** 330–34
[13] Yeung K Y M, Chee J, Yoon H, Song Y, Kong J and Ham D 2014 Far-infrared graphene plasmonic crystals for plasmonic band engineering *Nano Lett.* **14** 2479–84
[14] Yoon H, Yeung K Y M, Umansky V and Ham D 2012 A Newtonian approach to extraordinarily strong negative refraction *Nature* **488** 65–69
[15] Andress W F, Yoon H, Yeung K Y M, Qin L, West K, Pfeiffer L and Ham D 2012 Ultra-subwavelength two-dimensional plasmonic circuits *Nano Lett.* **12** 2272–77
[16] Ariel V and Natan A 2013 Electron effective mass in graphene *2013 Int. Conf. Electromagn. Adv. Appl. (ICEAA)* pp 696–98
[17] Novoselov K S, Geim A K, Morozov S V, Jiang D, Katsnelson M I, Grigorieva I V, Dubonos S V and Firsov A A 2005 Two-dimensional gas of massless dirac fermions in graphene *Nature* **438** 197–200
[18] Zhang Y, Tan Y W, Stormer H L and Kim P 2005 Experimental observation of the quantum hall effect and berry's phase in graphene *Nature* **438** 201–04
[19] Ju L *et al* 2011 Graphene plasmonics for tunable terahertz metamaterials *Nat. Nanotechnology* **6** 630–34
[20] Grigorenko A N, Polini M and Novoselov K S 2012 Graphene plasmonics *Nat. Photonics* **6** 749–58
[21] Zurita-Sánchez J R and Henkel C 2006 Lossy electrical transmission lines: Thermal fluctuations and quantization *Phys. Rev.* A **73** 063825